# Subwavelength Focusing of Light with Orbital Angular Momentum

Reinier W. Heeres*,† and Valery Zwiller

Kavli Institute of Nanoscience, Delft University of Technology, P.O. Box 5046, 2600 GA Delft, The Netherlands

 Supporting Information

ABSTRACT: The spatial structure of light with Orbital Angular Momentum, or "twisted light", closely resembles the shape of atomic wave functions. It could therefore make symmetry-forbidden transitions possible in quantum dots, or "artificial atoms". However, the vanishing intensity in the center of an OAM beam usually makes this effect weak. Here we show a plasmonic approach to focus OAM light to subwavelength dimensions using metallic nanoscale resonant optical antennas. This allows to increase the field intensity of OAM light at the typical dimensions of quantum dots to an intensity larger than a regular Gaussian beam, which corresponds to increasing the interaction strength by 3 orders of magnitude.
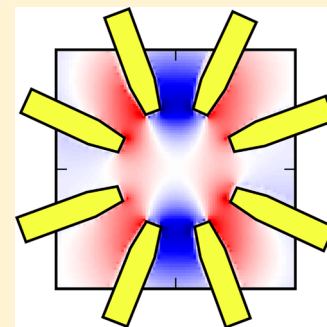
KEYWORDS: Orbital angular momentum; twisted light; plasmonic antennas; nanophotonics

The intrinsic angular momentum of light, associated with its polarization, has been known for a long time and can result in a measurable mechanical torque.[1] However, by manipulating the spatial structure of a light-beam, for example by using holograms[2] or spiral phase-plates,[3] light can also be made to "rotate" and carry an additional component of orbital angular momentum[4,5] (OAM). Not only can this OAM exert a torque,[6] it is also a fundamental property at the single-photon level, associated with an integer multiple of the basic unit of angular momentum, $\hbar$. The quantum nature of OAM has clearly been observed in quantum entanglement experiments.[7−9]

The donut-shaped intensity profile of OAM light is a result of the phase discontinuity, or vortex, at the center of the beam which causes the field-intensity to necessarily be zero there. OAM light can be described using Laguerre−Gaussian beams $LG_{pl}(r,\varphi)$ (see Methods), where l corresponds to the OAM number and p governs the number of radial maxima. We will be limiting our treatment to beams with $p = 0$. When focusing an OAM beam, its spatial extent is governed by diffraction. Figure 1a and b show the calculated field quadrature and intensity profiles of a focused beam with $l = 1$ and $l = 2$, respectively. An object of size $d \ll \lambda/2NA$, with λ the wavelength (900 nm) and NA the numerical aperture (here NA = 0.4), will lie completely in the low-intensity center and therefore interact with OAM light only very weakly. This effect becomes more pronounced for larger OAM number l, as the radius of maximum intensity scales with $\sqrt{l}$.[10]

To calculate the transition probability $P_{i \to f}$ for an electronic system to go from an initial state $|\Psi_i\rangle$ to a final state $|\Psi_f\rangle$, Fermi's golden rule is applied: $P_{i \to f} = |\langle \Psi_i | H_I | \Psi_f \rangle|^2 \rho_f(\omega)$, where H_I is the interaction Hamiltonian and $\rho_f(\omega)$ the density of final states. In case of optical transitions, H_I is given by $A(r) \cdot p$, with $A(r)$ the vector potential and p the momentum operator $(-i\hbar \nabla)$. Because the extent of the wave function is usually

much smaller than the wavelength one can typically apply the dipole approximation; i.e., the field can be considered constant over the integral and higher-order contributions that depend on the spatial variation of the vector potential can be ignored. In our case, this approximation does not hold for two reasons. First of all, in optical quantum dots, the wave function can span tens of nanometers, several orders of magnitude larger than typical atomic scales. This can result in measurable effects in for example the emission lifetime.[11] Second, by using a plasmonic antenna structure, much larger wave vectors can be accessed, and one is therefore not restricted to free-space propagating wave vectors which give the diffraction limit of $k_{max} = 2\pi/\lambda$. Although the integral for transition probabilities is hard to evaluate in general, one can predict which transitions will be allowed based on symmetry arguments.

The vector potential of an OAM beam can be written as $A(r,\varphi,z) = \varepsilon LG_{pl}(r,\varphi)e^{i(kz-\omega t)} + $ c.c., with ε the light polarization and z the direction of propagation. The electron wave functions in a disk-shaped circularly symmetric quantum dot, where the z-direction is most strongly confined, are approximately given by the LG functions in the (r, φ) plane.[12,13] The hole wave functions deviate significantly from this, but still keep their symmetry properties. Because the optical field and the wave functions are so similar, the overall symmetry of the transition probability integral $\int \Psi_i^*(r) A(r) \cdot (-i\hbar \nabla \Psi_f(r)) \, dr$ can now be modified by precisely choosing the spatial properties of the driving field.[14] This is in contrast to previous work about the breakdown of selection rules due to creation of large field-gradients in plasmonic structures.[15,16] The freedom of choosing the spatial structure of the incoming light beam profile allows,
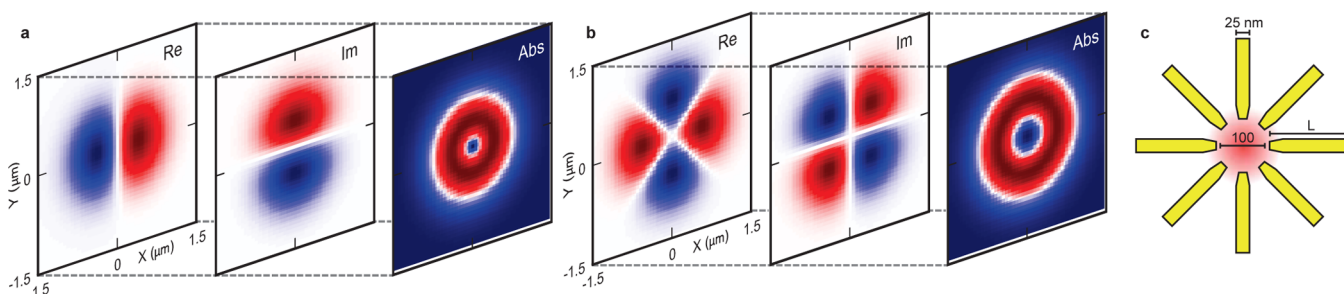
Figure 1. $l = 1$ and $l = 2$ Laguerre−Gaussian modes and antenna structure. (a) Field quadratures (indicated as real and imaginary part) and intensity of a Laguerre−Gaussian mode with $l = 1$, corresponding to a diffraction limited spot at 900 nm with a NA of 0.4. The donut intensity profile with vanishing intensity in the center is the biggest problem for coupling OAM light to microscopic structures. (b) same plots as in part a, but for an $l = 2$ mode. The center region of low intensity is larger than for an $l = 1$ mode. (c) the antenna geometry studied here: 8 gold rods, 25 nm wide, and 50 nm thick in a circular geometry. The aim is to focus OAM light in the central 100 nm wide region.
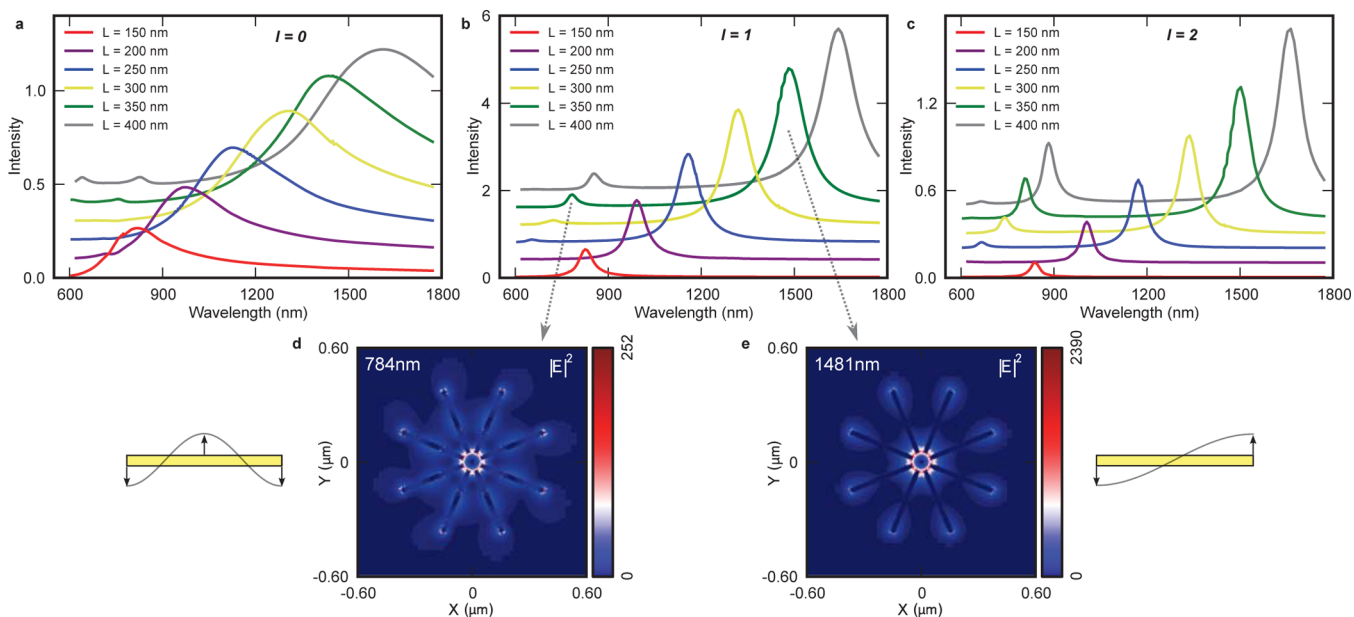

Figure 2. Wavelength-dependent antenna enhancement and resonant modes. (a) Integrated $|E|^2$ intensity within a circle of 48 nm radius around the center when illuminating several differently sized antennas of Figure 1c with a beam having $l = 0$, i.e., a normal Gaussian beam. Resonances are visible, but they have a very limited Q-factor of ∼3. Each curve is the result of 5 simulations with center wavelengths of 690, 860, 1070, 1320, and 1610 nm. The input beam is a diffraction limited spot with NA 0.6 at 1320 nm. (b) As in part a, but when illuminating the antennas with an $l = 1$ beam. The resonances are more pronounced and have a higher Q-factor of ∼10. (c) again as in part a but for an $l = 2$ beam. Resonances show an even higher Q-factor of ∼17. (d) Second order $l = 1$ mode for an antenna with $L = 350$ nm. This corresponds to each antenna arm being 1λ long. Three intensity maxima are visible, two at the ends of each rod and one in the center. (e) First order $l = 1$ mode for the same antenna; each arm is $(1/2)\lambda$ long. Only two intensity maxima are present at the rod ends.

for example, to selectively drive cylindrical quadrupole transitions that are dipole-forbidden by illuminating with $l = 1$ light (see Supporting Information for a more detailed analysis).

The antenna design we propose and study here is presented in Figure 1c. It consists of 8 circularly arranged strips of gold, each of them 25 nm wide and 50 nm thick, acting as dipole antennas.[17,18] A resonant antenna can confine a linearly polarized optical field spatially and enhance its intensity by several orders of magnitude. It has been shown that a system of 4 coupled antennas can reproduce any polarization state at the nanoscale.[19] Our system of 8 coupled antennas, however, has richer behavior that becomes clear when illuminating the structure with OAM light. This geometry is very different from so-called bull's eye structures, which have been shown to be able to transmit OAM light.[20]

We perform finite difference time domain (FDTD) simulations using Lumerical FDTD. At a distance of 50 nm above the antenna we position a circularly polarized source with $l = 0$ (a Gaussian beam), $l = 1$ or $l = 2$, and we monitor the resulting optical fields at midheight of the antenna structure. Since we are interested in enhancement of the absorbed energy in the central circle, we calculate the integral $\int|E|^2\,dA$ within a radius of 48 nm and plot the resulting intensity as a function of wavelength in Figure 2a−c. It is clear that for all instances of illumination the antenna shows one or more resonances. For the case of $l = 1$ illumination of an antenna with arm length of 350 nm we plot the two resonant modes in Figure 2, parts d and e. These correspond to the case where each antenna arm is half a wavelength long (Figure 2e, $\lambda = 1481$ nm) and one wavelength long (Figure 2d, $\lambda = 784$ nm) (the effective wavelength relevant for antennas is known to be shorter than the free-space wavelength[21]). It is interesting to note that the
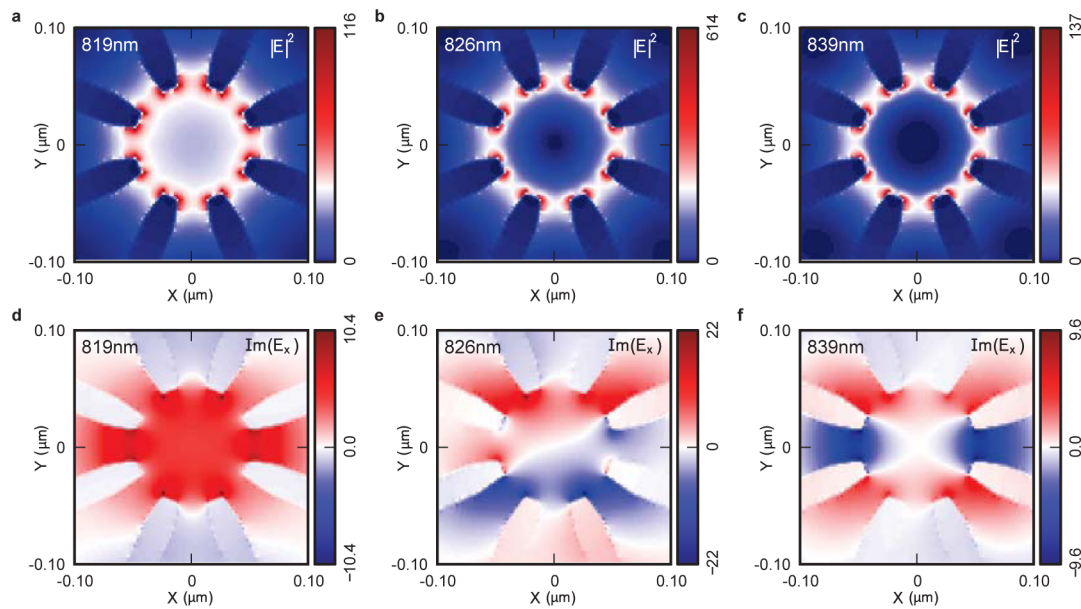
Figure 3. Confined OAM field profiles. (a−c) $|E|^2$ intensity profiles on resonance for an antenna with L = 150 nm for l = 0 (a), l = 1 (b), and l = 2 (c). Without OAM the intensity in the center is large whereas excitation with OAM light results in a vanishing intensity in the center. (d−f) Imaginary part of the E_x-component of the electromagnetic field for l = 0 (d), l = 1 (e), and l = 2 (f). The vanishing $|E|^2$ intensity in the center results from the phase relation corresponding to OAM light. A microscopic object in the center could therefore still be affected by the phase-vortex.
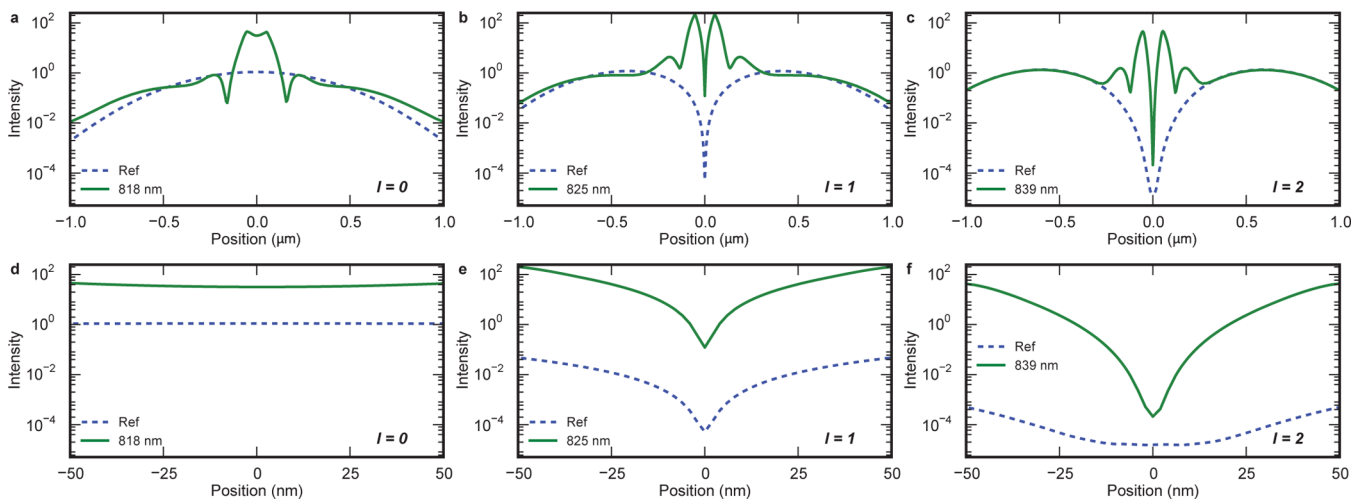
Figure 4. Confined OAM field intensity enhancement. (a−c) Line-cuts of the $|E|^2$ intensity profiles of the fields on resonance for an antenna with L = 150 nm in Figure 3a−c (solid green) for l = 0 (a), l = 1 (b) and l = 2 (c). A reference curve (dashed blue) indicates the field intensity without antenna structure and gives a good indication of the enhancement factor. (d−f) Zoom-ins of parts a−c.

interaction between the antenna arms results in much larger Q-factors when driven with a larger OAM number; this is usually related to a larger fraction of the resonant fields being present in the dielectrics and a smaller fraction in the lossy metals. Because of the lower optical losses in gold at longer wavelengths, the enhanced response becomes more pronounced at these longer wavelengths. We also observe a small red shift of the resonance with increasing OAM number.

In Figure 3a−c, we show a zoom-in of the antenna center (arm length L = 150 nm, $(1/2)\lambda$ resonance) and see that the field intensity is drastically enhanced there by at least 2 orders of magnitude. For l = 1 and l = 2 illumination there is a still a low intensity in the center; a requirement due to the phase-vortex. The crucial question now is whether the OAM spatial field profile is maintained at the nanoscale. Therefore, we plot one quadrature of the electric field in Figure 3d−f. As expected,

for a normal Gaussian beam (Figure 3d) the phase is constant within the antenna center. However, for l = 1 and l = 2 illumination the 2- and 4-lobed pattern associated with OAM light is still present with a high intensity (for all field components see Supporting Information, Figure S2 and S3). A quantum dot located in the center would therefore still be influenced by the spatially varying optical field. An antenna consisting of a larger number of arms, i.e. having higher symmetry, would be able to reproduce the field profile more faithfully. However, this would become impractical in terms of fabrication, so we have limited our treatment to 8 arms.

Finally, to better quantify the obtained intensity enhancement we plot line-cuts from Figure 3a−c on a logarithmic scale in Figure 4. From the zoomed-out images we see that the intensity profile is especially strongly modified for beams carrying OAM, with much higher intensities around the phase-

vortex at the origin ($r = 0$). From the zoomed-in images we learn that the OAM light intensity is even significant at the nanoscale: for $l = 1$, the intensity reaches that of a normal Gaussian beam at $r \sim 10$ nm; for $l = 2$, this occurs at $r \sim 20$ nm. These length-scales are close to the typical size of quantum dots.

The antenna structures we propose here would be very suitable for optical trapping[22] as well. In the $l = 0$, case they would deliver a high intensity localized trap that is cylindrically symmetric and can be used to trap dielectric particles with an index higher than their environment. Lossy and reflective particles, however, require an intensity *minimum* to be trapped.[23,24] Our antennas, in combination with $l = 1$ or $l = 2$ illumination, would be able to provide such a cylindrically symmetric trap on a much smaller length scale than available with free-space optics. The strongly enhanced confinement also results in a much stiffer trap, because the stiffness of a trap is proportional to the magnitude of the gradient. Because of both the increased intensity and the decreased spatial extent we find an enhancement of the field gradient magnitude of approximately 3.2×10^3 and 4.6×10^4 at $r = 10$ nm using $l = 1$ and $l = 2$ illumination respectively (see Supporting Information, Figure S4).

Our antenna structures provide a crucial enhancement of OAM light-field intensities at the nanoscale, and therefore open the way to explore interactions between OAM light and microscopic quantum systems. This could for example lead to efficient measurement of OAM number of a light beam and quantum information processing applications using optical quantum dots or Bose−Einstein condensates.[24]

Methods. *Laguerre−Gaussian Beams.* In the paraxial approximation the waist of a Laguerre−Gaussian beam is described by the field: $LG_{pl}(r,\varphi) = C(r\sqrt{2}/r_0)^{|l|}L_p^{|l|}((2r^2/r_0)\exp(-r^2/r_0^2))\exp(il\varphi)$ where C is a normalization constant, r_0 is the beam waist radius, r and φ the cylindrical coordinates and $L_p^{|l|}$ the generalized Laguerre polynomial of degree p and order $|l|$. The parameters p and l govern the number of radial maxima and azimuthal zero crossings respectively; we refer to l as the OAM number and only consider the case $p = 0$, i.e., only one radial maximum.

Simulation Details. Simulations are performed with Lumerical FDTD. The source field profile is a circularly polarized OAM beam corresponding to a diffraction limited spot at a wavelength of 1320 nm with an NA of 0.6. The meshing accuracy is set to 6 and in the central region of $150 \times 150 \times 60$ nm it has a $2 \times 2 \times 2$ nm resolution. The simulation is run with a dt stability factor of 0.9. Broadband results are obtained by performing several different simulations with center wavelengths of 690, 860, 1070, 1320, and 1610 nm.

■ ASSOCIATED CONTENT

Ⓢ Supporting Information

Transition probability symmetry considerations, additional simulation results (dispersion, full set of field profiles), and spontaneous emission enhancement estimation. This material is available free of charge via the Internet at http://pubs.acs.org.

■ AUTHOR INFORMATION

Corresponding Author
*(R.W.H.) E-mail: reinier@heeres.eu.

Present Address
†(R.W.H.) Departments of Applied Physics, Yale University, New Haven, CT 06511, United States.

Author Contributions
R.W.H. performed the simulations. R.W.H. and V.Z. thought of the concepts and wrote the manuscript together.

Notes
The authors declare no competing financial interest.

■ REFERENCES
(1) Beth, R. A. *Phys. Rev.* **1936**, *50*, 115−125.
(2) Heckenberg, N. R.; McDuff, R.; Smith, C. P.; White, A. G. *Opt. Lett.* **1992**, *17*, 221−223.
(3) Beijersbergen, M. W.; Coerwinkel, R. P. C.; Kristensen, M.; Woerdman, J. P. *Opt. Commun.* **1994**, *112*, 321−327.
(4) Allen, L.; Beijersbergen, M. W.; Spreeuw, R. J. C.; Woerdman, J. P. *Phys. Rev. A* **1992**, *45*, 8185−8189.
(5) Molina-Terriza, G.; Torres, J. P.; Torner, L. *Nat. Phys.* **2007**, *3*, 305−310.
(6) He, H.; Friese, M. E. J.; Heckenberg, N. R.; Rubinsztein-Dunlop, H. *Phys. Rev. Lett.* **1995**, *75*, 826−829.
(7) Mair, A.; Vaziri, A.; Weihs, G.; Zeilinger, A. *Nature* **2001**, *412*, 313−316.
(8) Dada, A. C.; Leach, J.; Buller, G. S.; Padgett, M. J.; Andersson, E. *Nat. Phys.* **2011**, *7*, 677−680.
(9) Leach, J.; Padgett, M. J.; Barnett, S. M.; Franke-Arnold, S.; Courtial, J. *Phys. Rev. Lett.* **2012**, *88*, 257901.
(10) Padgett, M. J.; Allen, L. *Opt. Commun.* **1995**, *121*, 36−40.
(11) Andersen, M. L.; Stobbe, S.; Sørensen, A. S.; Lodahl, P. *Nat. Phys.* **2010**, *7*, 215−218.
(12) Williamson, A. J.; Wang, L. W.; Zunger, A. *Phys. Rev. B* **2000**, *62*, 12963.
(13) Stier, O.; Grundmann, M.; Bimberg, D. *Phys. Rev. B* **1999**, *59*, 5688.
(14) Quinteiro, G. F.; Tamborenea, P. I. *Phys. Rev. B* **2009**, *79*, 155450.
(15) Cho, K.; Ohfuti, Y.; Arima, K. *Surf. Sci.* **1996**, *363*, 378−384.
(16) Jain, P. K.; Ghosh, D.; Baer, R.; Rabani, E.; Paul Alivisatos, A. *Proc. Natl. Acad. Sci. U.S.A.* **2012**, *109*, 8016−8019.
(17) Mühlschlegel, P.; Eisler, H. J.; Martin, O. J. F.; Hecht, B.; Pohl, D. W. *Science* **2005**, *308*, 1607−1609.
(18) Novotny, L.; Van Hulst, N. *Nat. Photonics* **2011**, *5*, 83−90.
(19) Biagioni, P.; Huang, J. S.; Duò, L.; Finazzi, M.; Hecht, B. *Phys. Rev. Lett.* **2009**, *102*, 256801.
(20) Wang, L. L.; Ren, X. F.; Yang, R.; Guo, G. C.; Guo, G. P. *Appl. Phys. Lett.* **2009**, *95*, 111111.
(21) Novotny, L. *Phys. Rev. Lett.* **2007**, *98*, 266802.
(22) Grier, D. G. *Nature* **2003**, *424*, 810−816.
(23) Ashkin, A.; Dziedzic, J. M. *Appl. Phys. Lett.* **1974**, *24*, 586−588.
(24) Andersen, M. F.; Ryu, C.; Cladé, P.; Natarajan, V.; Vaziri, A.; Helmerson, K.; Phillips, W. D. *Phys. Rev. Lett.* **2006**, *97*, 170406.